JACS
JOURNAL OF THE AMERICAN CHEMICAL SOCIETY

Communication

pubs.acs.org/JACS

Modulation of Phenol Oxidation in Cofacial Dyads

Bon Jun Koo,[†] Michael Huynh,[†] Robert L. Halbach,[†] JoAnne Stubbe,[‡] and Daniel G. Nocera*[,†]

[†]Department of Chemistry and Chemical Biology, Harvard University, 12 Oxford Street, Cambridge, Massachusetts 02138, United States

[‡]Department of Chemistry, Massachusetts Institute of Technology, 77 Massachusetts Avenue, Cambridge, Massachusetts 02139, United States

Supporting Information

ABSTRACT: The presentation of two phenols on a xanthene backbone is akin to the tyrosine dyad (Y_{730} and Y_{731}) of ribonucleotide reductase. X-ray crystallography reveals that the two phenol moieties are cofacially disposed at 4.35 Å. Cyclic voltammetry reveals that phenol oxidation is modulated within the dyad, which exhibits a splitting of one-electron waves with the second oxidation of the phenol dyad occurring at larger positive potential than that of a typical phenol. In contrast, a single phenol appended to a xanthene exhibits a two-electron process, consistent with reported oxidation pathways of phenols in acetonitrile. The perturbation of the phenol potential by stacking is reminiscent of a similar effect for guanines stacked within DNA base pairs.

Amino acid radicals play an essential role in the biochemistry of metabolism and catalysis.[1] Under physiological conditions, the generation and transport of amino acid radicals requires the coupling of a proton and an electron. The prominence of proton-coupled electron transfer (PCET) is arguably nowhere better exemplified than in *E. coli* class Ia ribonucleotide reductase (RNR), which catalyzes the reduction of nucleoside diphosphates to deoxynucleoside diphosphates.[2−4] RNR function relies on reversibly transferring a radical over a ~35 Å pathway between the amino acids, Y_{122} in β_2 and C_{439} in α_2 of *E. coli* class Ia RNR. The proposed pathway, for both forward and backward transfer, is β-$Y_{122} \rightleftarrows \beta$-$Y_{356} \rightleftarrows \alpha$-$Y_{731} \rightleftarrows \alpha$-$Y_{730} \rightleftarrows \alpha$-$C_{439}$.[1−3] Radical injection from β-Y_{356} into Y_{731} of the α_2 subunit is facilitated by the presence of adjacent Y_{730} (Figure 1).[5]

This result suggests that the dyad of two tyrosines does not simply provide two sequential radical pathway steps but that there is a collective property of two tyrosines, Y_{730} and Y_{731}. Whereas the oxidation kinetics of phenol, a redox active residue of tyrosine, have been thoroughly studied by photochemical, electrochemical, and radiochemical methods in the context of PCET,[6−12] the redox chemistry of π-stacked, cofacially aligned phenol dyads is unknown. In much the same way that the potential of guanines is perturbed by the presence of a neighboring guanine in DNA,[13,14] we wondered whether the potential of tyrosine is affected by the presence of a neighboring tyrosine.[15] To address this issue, we have prepared the models shown in Scheme 1. Two phenols may be cofacially positioned at a fixed distance from a 2,7-di-*tert*-butyl-4,5-di(4-hydroxyphenyl)-9,9-dimethylxanthene backbone (**DPX**). We have also developed control model systems **FPX** and **MPX** (Scheme 1) to allow the π-interaction between neighboring phenol units to be assessed. Electrochemical studies together with computational results establish that the phenol oxidation potential is perturbed within dyad **DPX** as compared to **FPX** and **MPX**. The perturbation in the formal reduction potential has significant implications to the PCET pathway of RNR.

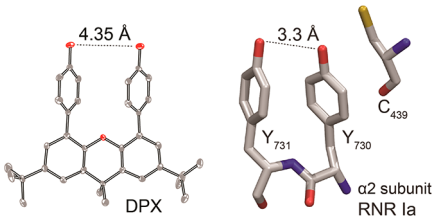

Figure 1. (Left) X-ray crystal structure of diphenol xanthene: oxygen (red) and carbon (gray); hydrogen omitted for clarity. (Right) RNR α_2 Y_{731} and Y_{730} from protein crystal structure 4R1R.

Scheme 1

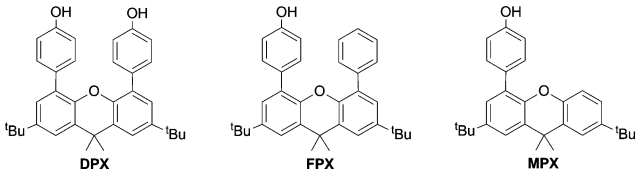

The syntheses and characterization of **DPX**, **FPX**, and **MPX** are presented in the Supporting Information. X-ray crystallography shows that two phenols are cofacially arranged as are Y_{731} and Y_{730} in RNR.[16] The O···O distance between phenols is 4.35 Å, and the centroid distance is 4.41 Å.

The cyclic voltammograms of the monophenol systems **FPX** and **MPX** in acetonitrile show a single peak (peaks IV and V, respectively, in Figure 2). Using the xanthene backbone peak as an internal one-electron (1-e$^-$) redox reference, both **MPX** and **FPX** show that the total charge passed during phenol oxidation corresponds to two-electron (2-e$^-$) processes. This peak amplitude is consistent with the well-established 2-e$^-$ ECE mechanism of phenol oxidation in CH_3CN (eq 1).[17−21]

The first oxidation yields a phenol radical cation ($\mathbf{F_1}$), which has a p$K_a \approx -5$ in acetonitrile, some ~20 pK_a units more acidic than the starting phenol. $\mathbf{F_1}$ deprotonates to a neutral phenol radical $\mathbf{F_2}$,[6] which is oxidized to phenoxium ($\mathbf{F_3}$) at a lower

Received: June 8, 2015
Published: August 25, 2015

DOI: 10.1021/jacs.5b05955
J. Am. Chem. Soc. 2015, 137, 11860−11863

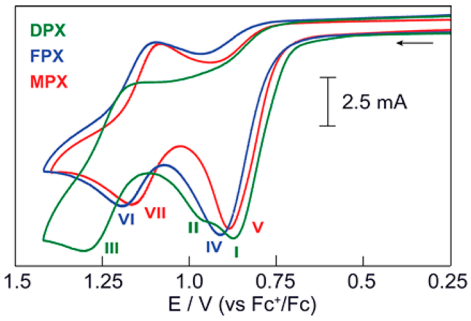

Figure 2. Cyclic voltammograms of **DPX** (green), **FPX** (blue), and **MPX** (red). All CVs were taken in 500 μM analyte, 0.1 M $TBAPF_6$ electrolyte in dry acetonitrile with a Pt working electrode, a Pt wire counter electrode, a Ag wire pseudo reference electrode, and referenced to Fc^+/Fc. The peak potentials of peaks I, II, IV, and V are 0.88, 0.98, 0.92, and 0.89 V, respectively. The $E_{1/2}$ potentials of peaks III, VI, and VII are 1.23, 1.13, and 1.12 V, respectively.

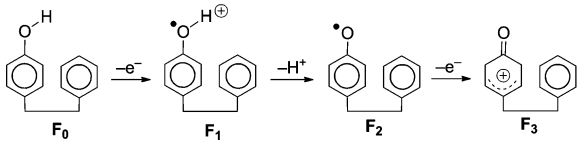

(1)

anodic potential than the initial oxidation, thus resulting a single peak for the total 2-e$^-$ process. A wave centered at 1.13 V (**FPX**, peak VI, Figure 2) is consistent with the 1-e$^-$ chemically reversible oxidation of the xanthene backbone; this oxidation does not interfere the phenol oxidation as shown by electrochemical analysis of various substituted xanthenes with phenyl analogues (Figure S3).

In contrast to the single 2-e$^-$ ECE wave for phenol oxidation in **MPX** (and **FPX**), the cyclic voltammetry (CV) of **DPX** shows two oxidation peaks at 0.88 and 0.98 V (peaks I and II in Figure 2, respectively), with the xanthene oxidation peak centered at 1.23 V. The total charge associated with the two waves corresponds to a 2-e$^-$ process, as references to the 1-e$^-$ xanthene wave. That two waves are separated in **DPX** indicates that the oxidation process of stacked phenols is perturbed in the dyad structure. We note that the peak potentials and ratio of peak amplitudes are invariant over a concentration range of 0.1−5 mM (Figure S5), confirming that the CV characteristics are not a result of an intermolecular interaction. CV features I and II exhibit a peak potential dependence, not originated from the ohmic drop, on scan rate of ~60 mV/decade (Figure 3a), suggesting the coupling of a chemical step with each electron-transfer step.[17] A computational analysis of related systems[22−24] suggests that the modulation of phenol oxidation, such as **DPX**, can originate from the H-bonding. Consistent with this contention is the disparate behavior of **DPX** and **FPX** despite similar π-aromatic electronic environments.

To investigate the effect of intramolecular H-bonding[25] on the redox properties of the dyad, CV was performed on **DPX** and **MPX** with titration of tetrabutylammonium hydroxide (TBAOH).[12] Base addition to **MPX** (Figure S8) results in a wave corresponding to phenolate oxidation at lower potentials (−0.3 to −0.6 V). For **DPX**, base addition affected peak I whereas peak II was largely unperturbed; these results suggest that peak II is a 1-e$^-$ oxidation process largely independent of a proton (Figure 3b) whereas peak I is more intimately related to the proton. In line with these observations, peak I shifts to −0.25 V with the addition of base, in accordance with the shift in

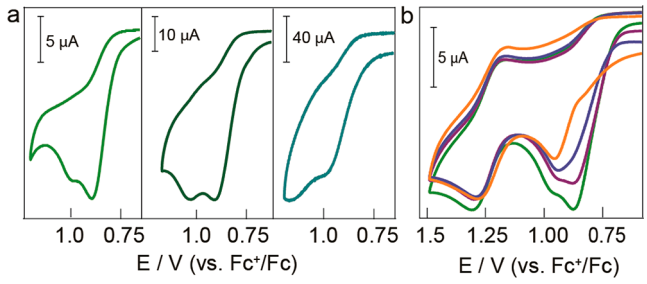

Figure 3. Scan rate dependence of **DPX**. (a) Peak I and peak II amplitudes at 0.1 (left, green), 1 (middle, dark green), and 10 V/s (right, emerald). (b) Change in **DPX**'s peaks I and II with TBAOH titration of 0 (green), 0.5 (violet), 1.0 (blue), and 2.0 equiv (orange).

Scheme 2. Postulated Oxidation Pathways of DPX

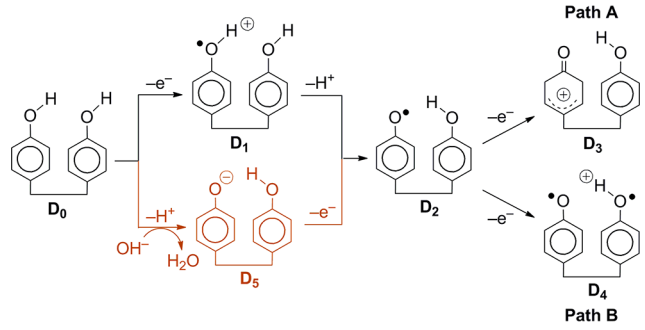

potential resulting for the 1-e$^-$ oxidation of phenolate to phenoxy radical (Figure S7).[18] The first 1-e$^-$ oxidation of **DPX** in base is described by $\mathbf{D_5}$ to $\mathbf{D_2}$ in Scheme 2. In base, phenol $\mathbf{D_0}$ is deprotonated to phenolate $\mathbf{D_5}$, which is the species that is oxidized by one electron to produce phenoxy radical $\mathbf{D_2}$. Given peak II is proton independent (base <2 equiv), the subsequent oxidation of $\mathbf{D_2}$ proceeds from the phenoxy radical. In the absence of base, $\mathbf{D_2}$ is produced by the direct 1-e$^-$ oxidation (peak I in Figure 2) of $\mathbf{D_0}$ to produce phenol radical cation species ($\mathbf{D_1}$ in Scheme 2) followed by fast deprotonation to yield phenol radical ($\mathbf{D_2}$).[6,26] A scan rate dependent shift of the peak I potential indicates involvement of a chemical step, which is consistent with deprotonation accompanying the conversion of $\mathbf{D_0}$ to $\mathbf{D_2}$. Further oxidation of $\mathbf{D_2}$ may follow two paths, indicated by Paths A and B. In Path A, the 2-e$^-$ oxidation process results in one phenoxium and an intact phenol unit ($\mathbf{D_3}$) and in Path B, $\mathbf{D_4}$ is produced. Computation shows that biradical $\mathbf{D_4}$ (triplet) is considerably more stable than $\mathbf{D_3}$ (vide infra). Spectroelectochemistry shows that this product is unstable, and it cannot be isolated. Because the standard potential of the second oxidation step (from $\mathbf{D_2}$ to $\mathbf{D_4}$) is greater than that of the first oxidation step (from $\mathbf{D_1}$ to $\mathbf{D_2}$), the phenol oxidation peaks are separated. The separation of ~100 mV occurs about the potential that is observed for the single wave oxidation of **FPX**. Note that the overall ECE mechanism is similar for both **DPX** and **FPX**. However, the presence of the H-bonding from the second phenol in **DPX** stabilizes the first oxidation with respect to the ensuing oxidation, thus resulting in a split peak in the CV.

Computational methods were employed to further analyze the mechanistic pathways of Scheme 2. Density functional theory (DFT) calculations were performed with Gaussian 09, where all structures were optimized in the gas phase at the B3LYP/6-311+G(d,p) level of theory with Grimme's D3 dispersion correction[27] and verified by the absence of imaginary vibrational

DOI: 10.1021/jacs.5b05955
J. Am. Chem. Soc. 2015, 137, 11860−11863

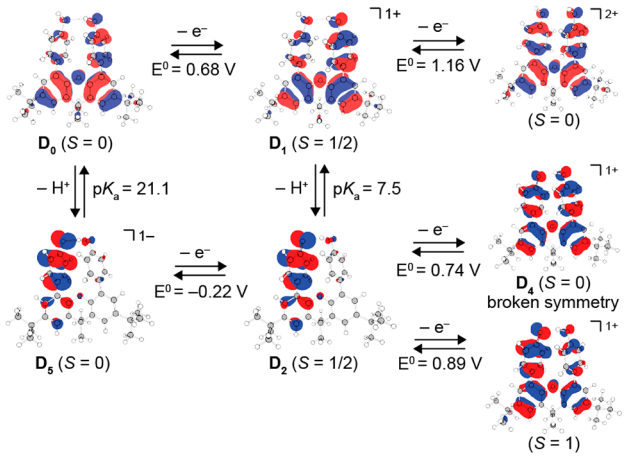

Figure 4. Calculated reduction potentials and pK_a's for **DPX**. Bolded labels correspond to **DPX** states defined in Scheme 2. Molecular orbitals depict the HOMO for singlet (S = 0) states and the "spin density" SOMO for doublet and triplet states (S = 1/2 and 1, respectively). In addition, the "spin density" SOMO is shown for the $\mathbf{D}_4$ state of **DPX** and is predicted to be a "broken symmetry" singlet. The triplet ground state of $\mathbf{D}_4$ is more stable than the singlet. Explicit spin density plots for the second oxidation from $\mathbf{D}_2$ is shown in Figure S9.

frequencies as local minima. Solvation free energies in acetonitrile were computed by the SMD polarizable continuum model,[28] which includes corrections for non-electrostatic interactions. From these gas-phase free energies, solution-phase reaction free energies were calculated for each step of the mechanism using the Born–Haber cycle.[29] The free energies were converted to reduction potentials[29−32] or pK_a's[32−36] by using appropriate reference reactions to account for systematic error in the computations, primarily stemming from the calculation of solvation and thermal energies as well as functional and basis set limitations. For the phenol systems, oxidation of the xanthene backbone (reversible peak III in Figure 2) served as an internal reference between calculated and experimental reduction potentials, while the isodesmic reaction between the phenol systems and 4-*tert*-butylphenol was employed for improving the accuracy of calculated pK_a's.

The calculated electronics and energetics of the phenol systems (Figure 4 for **DPX**, Figures S9 and S10 for **FPX** and **MPX**, respectively) are consistent with their proposed mechanistic pathways (Scheme 2). First, the calculated reduction potentials for all three model systems agree with an ECE mechanism. The first oxidation facilitates the deprotonation of a phenol unit, where the calculated first pK_a decreases by 13–20 units to p$K_a \approx 7$ in acetonitrile, which establishes a minor equilibrium of singly deprotonated phenol systems. This then enables the second oxidation to occur at similar potentials as the first oxidation, which is consistent with the integration of the first oxidation wave to a 2-e$^-$ process in the CVs of the model systems (peaks I/II, IV, and V in Figure 2). In particular, DFT calculates a larger first and second reduction potential difference for **DPX** of ~60 mV compared to that of **FPX** and **MPX** (of 10–20 mV gap), which explains why **DPX** exhibits split peaks (I and II in Figure 2) in CVs whereas **FPX** and **MPX** only display a single peak (IV and V in Figure 2) as the second oxidation closely overlaps with the first oxidation. In contrast, calculations show that without the intermediate deprotonation step, the second oxidation of the phenols occurs ~500–700 mV to higher anodic potential, which supports the assignment that the second oxidation is the subsequent oxidation of deprotonated product. Similarly, when the phenol are deprotonated prior to any oxidations (by the addition of base), the calculations predict a drastic ~900–1200 mV cathodic shift of the first reduction potential that is observed in the CVs of base-titrated phenol systems (Figures S7 and S8), where the first oxidation now occurs from −0.25 to −0.30 V vs Fc^+/Fc. Direct comparison of calculated to experimental reduction potentials is discouraged because DFT reports reversible potentials while CVs show only peak potentials for oxidation of the phenol systems—the experimental reversible reduction potentials are unknown. Notwithstanding, the PCET effects of oxidations and deprotonations on the phenol systems are readily reproduced by computation.

Analysis of calculated molecular orbitals and spin densities provides a qualitative view of the electronic interaction occurring in the phenol model systems, and in particular, suggests that the second oxidation of **DPX** is distributed on the adjacent phenol moiety (Path B in Scheme 2). In all phenol systems, visualization of the spin density via the corresponding singly occupied molecular orbital (SOMO) shows that the first oxidation results in a radical cation that is distributed on a single phenol with minor extension of spin to the xanthene backbone (e.g., see the $\mathbf{D}_1$ state for **DPX** in Figure 4). Upon deprotonation, the radical cation becomes primarily localized on the single phenol unit, which is consistent with Scheme 2 (i.e., $\mathbf{D}_2$ and $\mathbf{F}_2$ in Scheme 2 and eq 1, respectively). The second oxidation after deprotonation favors the singlet (phenoxium cation) over the triplet (biradical) state by ~4–6 kcal/mol. For **FPX** and **MPX**, the spin density of this singlet state was zero, demonstrating that the second oxidation removes an electron from the same phenol unit that had initially undergone the first oxidation and deprotonation (e.g., $\mathbf{F}_3$ in eq 1). Conversely, for **DPX**, the same singly deprotonated, doubly oxidized singlet state exhibited significant spin density of opposing character on each of the phenol units (triplet biradical $\mathbf{D}_4$ in Figure 4 and Scheme 2, and Figure S9), signifying the presence of "broken symmetry" where the α and β spins of the highest occupied molecular orbital (HOMO) are localized as antiferromagnetically coupled radical cations on each of the phenol units, respectively.[37,38] Thus, a formal singlet spin state is preserved while retaining local diradical character. These calculations suggest that the biradical is stabilized by the coupling of phenol rings (via H-bonding) and predict that Path B in Scheme 2 describes the second oxidation of **DPX**. However, we caution that spin-density derived from unrestricted DFT may not always be accurate, especially for long-range interactions, and must be qualitatively interpreted.[39]

In summary, we have shown that oxidation of a phenol moiety is perturbed when it resides within a cofacial dyad. The stacked phenol units of **DPX** display a cooperative ECE oxidation mechanism that is unique from that of monophenol analogues (**FPX** and **MPX**). Unlike the ECE mechanism of **FPX** and **MPX** in acetonitrile, **DPX** showed two 1-e$^-$ oxidations. The presence of broken symmetry in **DPX**, but not in **FPX** and **MPX**, indicates the importance of the hydroxide group on the adjacent phenol, which aids in electronically modifying electron density (and by extension, the radical) within the dyad and also assists in coupling the two units via H-bonding site. Consequently, the strong coupling of phenols in **DPX** results in each phenol not behaving as independent redox units but rather as a cooperative redox entity where removal of a second electron from the system occurs at a higher anodic potential than that of the first oxidation. These results have implications to the radical transport pathway in RNR. Comparison of **DPX** to **FPX** shows that the potential of

DOI: 10.1021/jacs.5b05955
J. Am. Chem. Soc. 2015, 137, 11860–11863

phenol is perturbed by ~50 mV (peak potential difference between the first oxidation of **DPX** and **FPX**). We note that the entire redox ramp for radical transport in RNR—from Y356 to Y731—is estimated to be ~100 mV uphill.[40] Thus, the perturbation of the oxidation of the phenol moiety within the dyad would represent significant tuning of the formal reduction potential within the radical transport pathway of RNR. Both statistical and computational analyses suggest that pairs of aromatic amino acids with a centroid distance range of 3.4−7 Å, like that of the Y_{730} and Y_{731} dyad, are likely to play crucial functions in substrate recognition, structure, and catalysis in proteins.[41] Various aspects of through-space π-interactions have been investigated for their effects on charge transfer, pK_a and energy transfer.[42−44] We now show that the redox properties of the phenol moiety of tyrosine will be affected by cofacial disposition within a dyad, thus highlighting the fidelity of the RNR radical transport pathway. Further investigation on the energetics and mechanism of **DPX** oxidation in terms of H-bonding and π-interaction will afford greater insight into how these non-covalent interactions are being used in enzyme systems like RNR.

■ ASSOCIATED CONTENT

Supporting Information

The Supporting Information is available free of charge on the ACS Publications website at DOI: 10.1021/jacs.5b05955.

Experimental, synthetic, and crystal structure details; additional CVs, UV/vis spectra, spin density plots, calculated reduction potential and pK_a values for **FPX** and **MPX**, and DFT optimized structures (PDF)
X-ray crystallographic data for **DPX** (CIF)

■ AUTHOR INFORMATION

Corresponding Author

*dnocera@fas.harvard.edu

Notes

The authors declare no competing financial interest.

■ ACKNOWLEDGMENTS

We thank Drs. Andrew M. Ullman, Daniel K. Bediako, and Shaw Huang for helpful discussions. The National Institutes of Health (GM047274 (D.G.N.) and GM029595 (J.S.)) provided funding for this research. The computations in this paper were run on the Odyssey cluster supported by the FAS Division of Science, Research Computing Group at Harvard University.

■ REFERENCES

(1) Stubbe, J.; Nocera, D. G.; Yee, C. S.; Chang, M. C. Y. *Chem. Rev.* **2003**, *103*, 2167.
(2) Minnihan, E. C.; Nocera, D. G.; Stubbe, J. *Acc. Chem. Res.* **2013**, *46*, 2524.
(3) Uhlin, U.; Eklund, H. *Nature* **1994**, *370*, 533.
(4) Nordlund, P.; Eklund, H. *J. Mol. Biol.* **1993**, *232*, 123.
(5) (a) Holder, P. G.; Pizano, A. A.; Anderson, B. L.; Stubbe, J.; Nocera, D. G. *J. Am. Chem. Soc.* **2012**, *134*, 1172. (b) Pizano, A. A.; Olshansky, L.; Holder, P. G.; Stubbe, J.; Nocera, D. G. *J. Am. Chem. Soc.* **2013**, *135*, 13250.
(6) Warren, J. J.; Winkler, J. R.; Gray, H. B. *FEBS Lett.* **2012**, *586*, 596.
(7) Weinberg, D. R.; Gagliardi, C. J.; Hull, J. F.; Murphy, C. F.; Kent, C. A.; Westlake, B. C.; Paul, A.; Ess, D. H.; McCafferty, D. G.; Meyer, T. J. *Chem. Rev.* **2012**, *112*, 4016.
(8) Markle, T. F.; Rhile, I. J.; Mayer, J. M. *J. Am. Chem. Soc.* **2011**, *133*, 17341.
(9) Moore, G. F.; Hambourger, M.; Kodis, G.; Michl, W.; Gust, D.; Moore, T. A.; Moore, A. L. *J. Phys. Chem. B* **2010**, *114*, 14450.
(10) Bonin, J.; Routier, M. *Artif. Photosynth.* **2013**, *1*, 6.
(11) Costentin, C.; Robert, M.; Savéant, J.-M.; Tard, C. *Angew. Chem.* **2010**, *122*, 3891.
(12) Costentin, C.; Robert, M.; Savéant, J.-M.; Tard, C. *Phys. Chem. Chem. Phys.* **2011**, *13*, 5353.
(13) Sistare, M. F.; Codden, S. J.; Heimlich, G.; Thorp, H. H. *J. Am. Chem. Soc.* **2000**, *122*, 4742.
(14) Stemp, E. D. A; Arkin, M. R.; Barton, J. K. *J. Am. Chem. Soc.* **1997**, *119*, 2921.
(15) Niemz, A.; Rotello, V. M. *Acc. Chem. Res.* **1999**, *32*, 44.
(16) Nick, T. U.; Lee, W.; Koßmann, S.; Neese, F.; Stubbe, J.; Bennati, M. *J. Am. Chem. Soc.* **2015**, *137*, 289.
(17) Savéant, J.-M. *Elements of Molecular and Biomolecular Electrochemistry: An Electrochemical Approach to Electron Transfer Chemistrry*; John Wiley: Hoboken, NJ, 2006.
(18) Richards, J. A.; Whitson, P. E.; Evans, D. H. *J. Electroanal. Chem. Interfacial Electrochem.* **1975**, *63*, 311.
(19) Costentin, C.; Louault, C.; Robert, M.; Savéant, J.-M. *J. Am. Chem. Soc.* **2008**, *130*, 15817.
(20) Costentin, C.; Louault, C.; Robert, M.; Savéant, J.-M. *Proc. Natl. Acad. Sci. U. S. A.* **2009**, *106*, 18143.
(21) Bonin, J.; Costentin, C.; Louault, C.; Robert, M.; Savéant, J.-M. *J. Am. Chem. Soc.* **2011**, *133*, 6668.
(22) Kaila, V. R. I.; Hummer, G. *J. Am. Chem. Soc.* **2011**, *133*, 19040.
(23) Mayer, J. M.; Hrovat, D. A.; Thomas, J. L.; Borden, W. T. *J. Am. Chem. Soc.* **2002**, *124*, 11142.
(24) DiLabio, G. A.; Johnson, E. R. *J. Am. Chem. Soc.* **2007**, *129*, 6199.
(25) Bonin, J.; Costentin, C.; Robert, M.; Savéant, J.-M.; Tard, C. *Acc. Chem. Res.* **2012**, *45*, 372.
(26) Bordwell, F. G.; Cheng, J. *J. Am. Chem. Soc.* **1991**, *113*, 1736.
(27) Grimme, S.; Antony, J.; Ehrlich, S.; Krieg, H. *J. Chem. Phys.* **2010**, *132*, 154104.
(28) Marenich, A. V.; Cramer, C. J.; Truhlar, D. G. *J. Phys. Chem. B* **2009**, *113*, 6378.
(29) Cramer, C. J. In *Essentials of Computational Chemistry Theories and Models*; John Wiley: West Sussex, England, 2004; p 429.
(30) Baik, M.-H.; Friesner, R. A. *J. Phys. Chem. A* **2002**, *106*, 7407.
(31) Konezny, S. J.; Doherty, M. D.; Luca, O. R.; Crabtree, R. H.; Soloveichik, G. L.; Batista, V. S. *J. Phys. Chem. C* **2012**, *116*, 6349.
(32) Solis, B. H.; Hammes-Schiffer, S. *Inorg. Chem.* **2011**, *50*, 11252.
(33) Ho, J.; Coote, M. L. *J. Chem. Theory Comput.* **2009**, *5*, 295.
(34) Alongi, K. S.; Shields, G. C. *Annu. Rep. Comput. Chem.* **2010**, *6*, 113.
(35) Casasnovas, R.; Fernández, D.; Ortega-Castro, J.; Frau, J.; Donoso, J.; Muñoz, F. *Theor. Chem. Acc.* **2011**, *130*, 1.
(36) Sastre, S.; Casasnovas, R.; Muñoz, F.; Frau, J. *Theor. Chem. Acc.* **2013**, *132*, 1310.
(37) Sinnecker, S.; Neese, F.; Noodleman, L.; Lubitz, W. *J. Am. Chem. Soc.* **2004**, *126*, 2613.
(38) Neese, F. *J. Phys. Chem. Solids* **2004**, *65*, 781.
(39) (a) Perdew, J. P.; Ruzsinszky, A.; Constantin, L. A.; Sun, J.; Csonka, G. I. *J. Chem. Theory Comput.* **2009**, *5*, 902. (b) Boguslawski, K.; Jacob, C. R.; Reiher, M. *J. Chem. Theory Comput.* **2011**, *7*, 2740.
(40) Yokoyama, K.; Smith, A. A.; Corzilius, B.; Griffin, R. G.; Stubbe, J. *J. Am. Chem. Soc.* **2011**, *133*, 18420.
(41) (a) Grimme, S. *Angew. Chem., Int. Ed.* **2008**, *47*, 3430. (b) McGaughey, G. B.; Gagné, M.; Rappé, A. K. *J. Biol. Chem.* **1998**, *273*, 15458.
(42) Holmlin, R. E.; Dandliker, P. J.; Barton, J. K. *Angew. Chem., Int. Ed. Engl.* **1997**, *36*, 2714.
(43) Cozzi, F.; Cinquini, M.; Annuziata, R.; Siegel, J. S. *J. Am. Chem. Soc.* **1993**, *115*, 5330.
(44) Cadman, C. J.; Croft, A. K. *Beilstein J. Org. Chem.* **2011**, *7*, 320.

DOI: 10.1021/jacs.5b05955
J. Am. Chem. Soc. 2015, 137, 11860−11863